Supplementary Information

Structural, Dynamic, and Diffusion Properties of $Li_6(PS_4)SCl$ Superionic Conductor from Molecular Dynamics Simulations

Tridip Das, Boris V. Merinov,* Moon Young Yang, and William A. Goddard III*

Materials and Process Simulation Center, MC 139-74, California Institute of Technology, Pasadena, California 91125, United States

*Corresponding author email: merinov@caltech.edu and wag@caltech.edu

List of Figures and Tables:

Figure S1. (a) DFT predicted P-S bond length distribution from energy minimized structure (b) LAMMPS MD predicted P-S bond length distribution from the UFF structural minimization. 2

Figure S2. (a) Density, (b) volume, (c) temperature, and (d) pressure fluctuations in the 20 ns NPT simulation at 293 K. 3

Figure S3. (a) MSD of the different species calculated from the 20 ns MD simulations on $Li_6(PS_4)SCl$ at 273, 293, 325, 350, 400, and 500 K. The dotted blue lines have a slope of 1 represented by the dash-dotted black lines. (b) Results from application of a constant electric field of 0.1 V/nm. Average velocity of each ion type at room temperature (293 K) *vs.* time. 4

Figure S4. Mean square displacements (MSD) of the different species calculated from the 20 ns MD simulation on $Li_6(PS_4)SCl$ at 350 K. 5

Figure S5. The log plots of the Li-ion conductivity multiplied by temperature (σT) vs. temperature reported in literature. 5

Figure S6. Trajectories of P and S atoms of PS_4 tetrahedra indicating rotation of the PS_4 units at different temperatures: (a) one rotation at 273 K, (b) two at 293 K, (c) eight at 325 K, and (d) eighteen at 350 K. 6

Figure S7. Ion diffusion in $Li_7(PS_4)S_2$ - mean square displacement (MSD) of the species vs. time at room temperature (293 K). 7

Figure S8. (a) Trajectories of 10 farthest moving Li-ions without electric field at 293 K. (b) The trajectories of 10 farthest moving Li-ions under the *x*-directional electric field of 0.01 V/Å. 8

Figure S9. Trajectories of the species in $Li_6(PS_4)SCl$ under different electric field strengths at room temperature (293 K). 8

Figure S10. Trajectories of 10 farthest diffusing Li-ions over 20 ns under the 0.01 V/Å electric field applied along the (a) *x*, (b) *y*, and (c) *z* directions. 9

Figure S11. (a) the vibrational DoS contribution from the PS_4 tetrahedra, and (b) the molar volume predicted from one phase dynamics calculations. 11

Table S1. Summary of experimental measurements: Li-ionic conductivity in $Li_6(PS_4)SCl$ at room temperature (298 K) and the activation energy. 12

Table S2. UFF parameters used in the LAMMPS calculations. 13

Table S3. Atomic charge comparison from LAMMPS scaled charges *vs.* DFT calculated DDEC6 charges. 14

Section S1: DFT calculation setup

We used VASP (Vienna *Ab initio* Simulation Package, v5.4.4) for all density functional theory (DFT) computations on the ground state (0 K).[1,2] The Projector-augmented-wave (PAW) potentials with valence configurations of $1s^2 2s^1$ for Li, $2s^2 2p^3$ for P, $2s^2 2p^4$ for S, and $2s^2 2p^5$ for Cl was applied to describe the valence electrons.[3,4] The Perdew, Burke, and Ernzerhof (PBE) flavor of the generalized gradient approximation (GGA) functional was applied to describe the exchange-correlation potentials of the constituting elements.[5,6] In addition, we included the Grimme D3 vdW correction (PBE-D3) with the Becke-Johnson parameters. The accuracy of the electronic calculations was within 1 μeV. A single point energy calculation was performed to test the convergence of cut-off energy and *k*-points for input lattices. We concluded from the *k*-mesh calculations that a *k*-spacing of 0.2 $Å^{-1}$ was sufficient for the required accuracy of 1 meV/atom when the cutoff energy was set to 500 eV. Ionic relaxations were performed until the Hellmann-Feynman force on each atom reached an order of 10 meV/ Å.[7,8]

Section S2: DDEC6 calculated charges and charge assignment on Li and other species

DDEC6 method[9] was employed in the literature to accurately predict NAC (net atomic charges) on charged species. Here we used the same method to calculate the partial charge on all the ionic species in the system (Table S3). The calculated charge was later scaled to with charge on Li to accurately predict the room temperature Li-ion diffusivity obtained from experiments. It was observed with charge of +0.4 and +0.5 on Li-ion the ionic diffusivity is respectively higher or lower than experimental diffusivity at room temperature but a charge of +0.45 gives more accurate prediction.

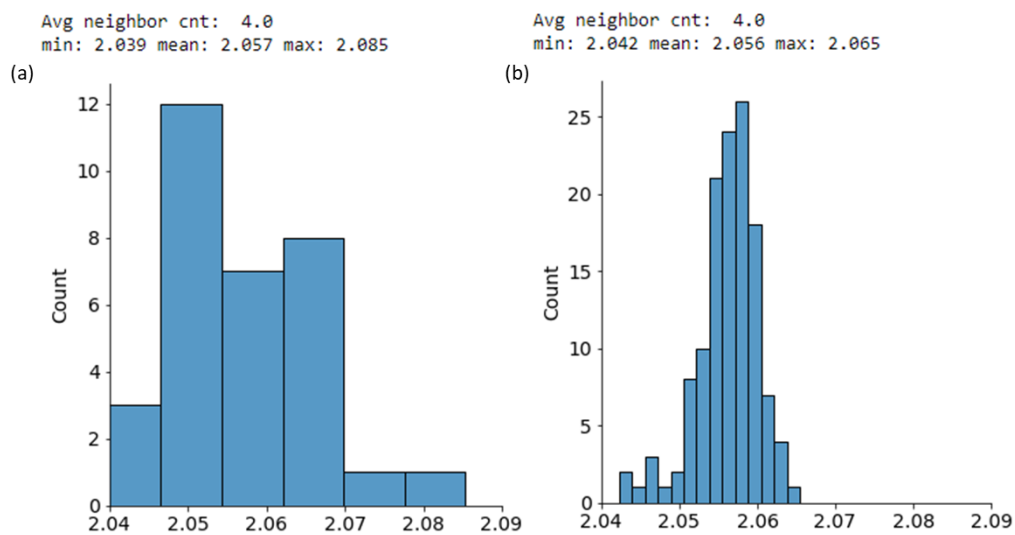

Figure S1. (a) DFT predicted P–S bond length distribution from energy minimized structure (b) LAMMPS MD predicted P–S bond length distribution from the UFF structural minimization.

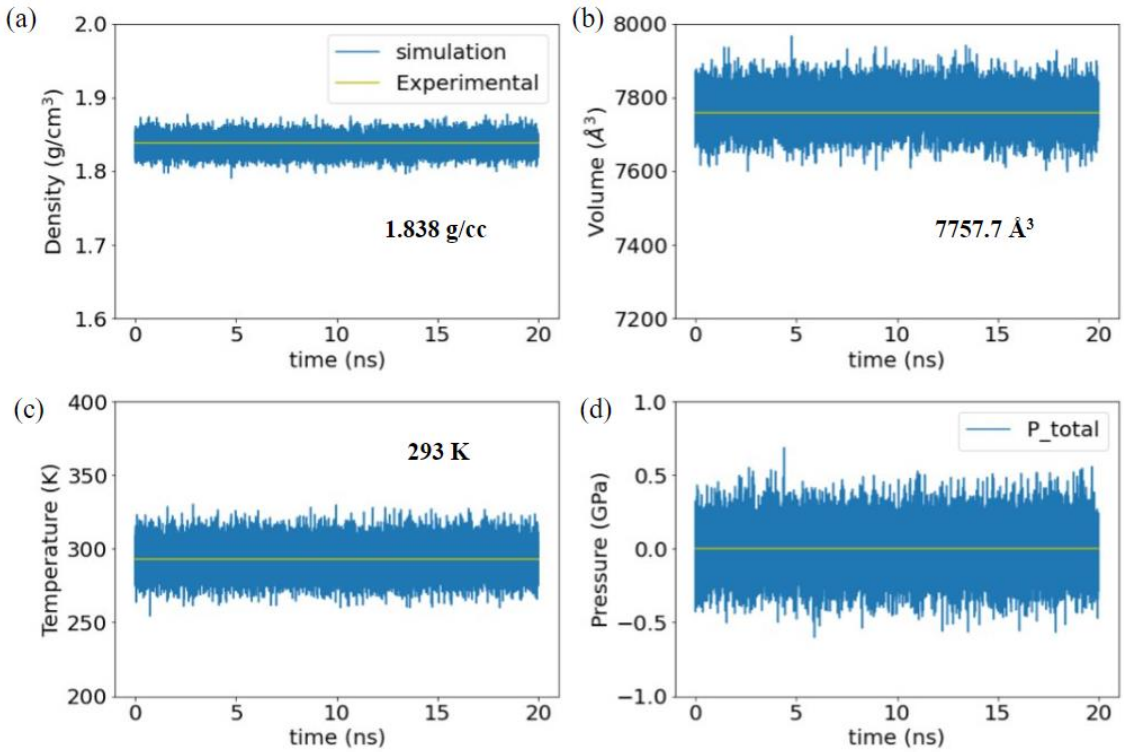

Figure S2. (a) Density, (b) volume, (c) temperature, and (d) pressure fluctuations in the 20 ns NPT simulation on $Li_6(PS_4)SCl$ at 293 K. The yellow line shows the experimental target.

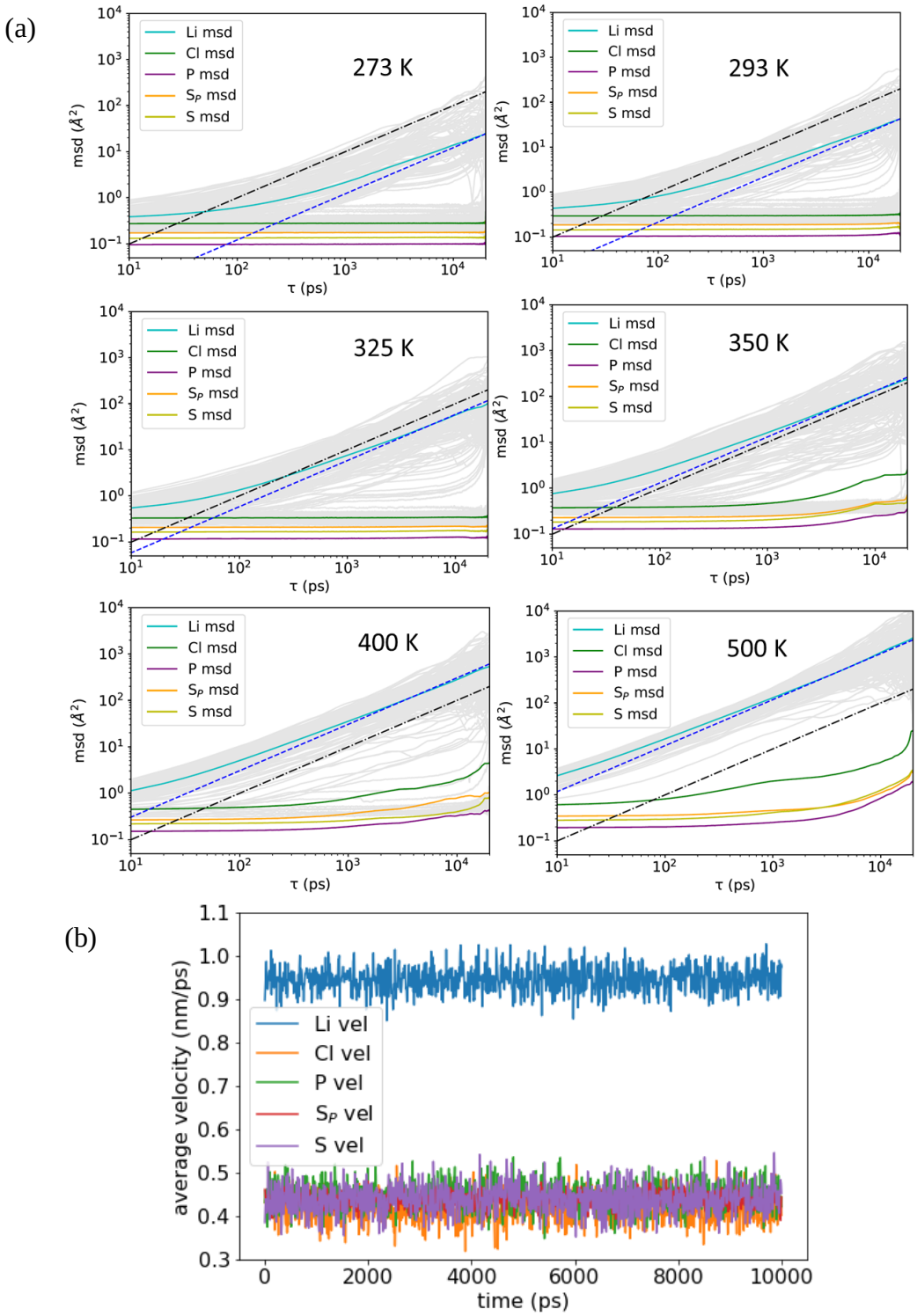

Figure S3. (a) MSD of the different species calculated from the 20 ns MD simulations on $Li_6(PS_4)SCl$ at 273, 293, 325, 350, 400, and 500 K. The dotted blue lines have a slope of 1 represented by the dash-dotted black lines. (b) Results from application of a constant electric field of 0.1 V/nm. Average velocity of each ion type at room temperature (293 K) *vs.* time.

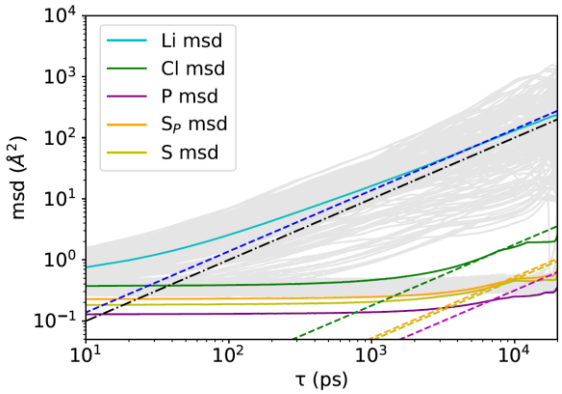

Figure S4. Mean square displacements (MSD) of the different species calculated from the 20 ns MD simulation on $Li_6(PS_4)SCl$ at 350 K. The dotted lines have a slope of 1 represented by the dash-dotted black line. The Li-ion diffusivity (2.1×10^{-7} cm^2/s) is by 2-3 orders of magnitude higher than that of the anions (S – 8.0×10^{-10} cm^2/s, Cl – 3.0×10^{-9} cm^2/s, P – 5.2×10^{-10} cm^2/s, and S_P – 8.7×10^{-10} cm^2/s). A transference number for the Li-ions was calculated as 0.98.

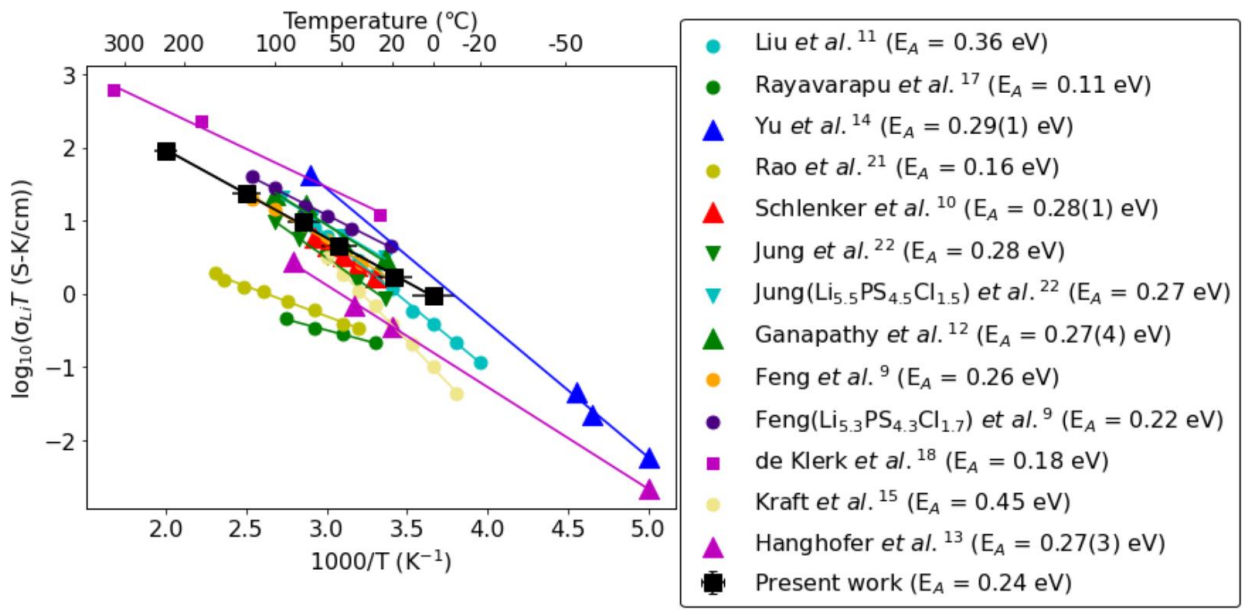

Figure S5. The log plots of the Li-ion conductivity multiplied by temperature (σT) vs. temperature reported in literature. Note that our calculations lead to a comparable slope with E_a = 0.24 eV. Filled circles represent the experimental EIS data. Filled triangles represent the experimental NMR data. Filled squares represent computationally predicted data. Computationally predicted activation energy should be compared with the activation energy from NMR measurement due to no impact of grain boundaries and electrode contacts on the bulk conductivity measurement and minimal variation, 0.27(4) − 0.29(1) eV.

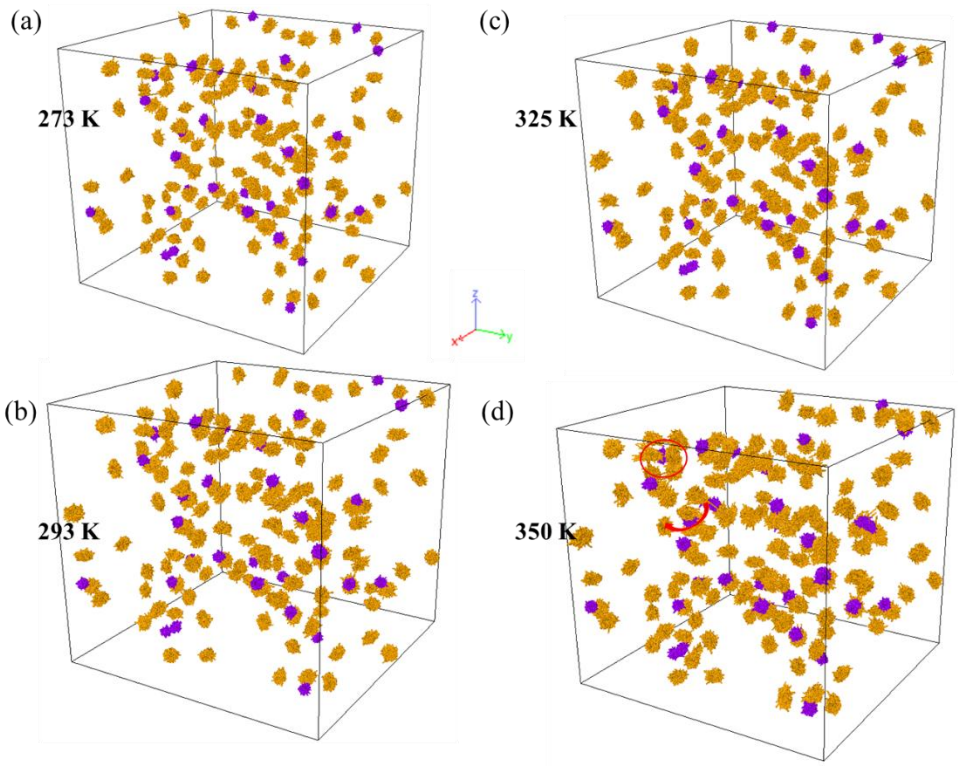

Figure S6. Trajectories of P (purple) and S (orange) atoms of PS_4 tetrahedra indicating rotation of the PS_4 units at 350 K (d). No rotation of PS_4 units were observed at (a) 273 K, (b) 293 K, and (c) 325 K for 20 ns of simulations.

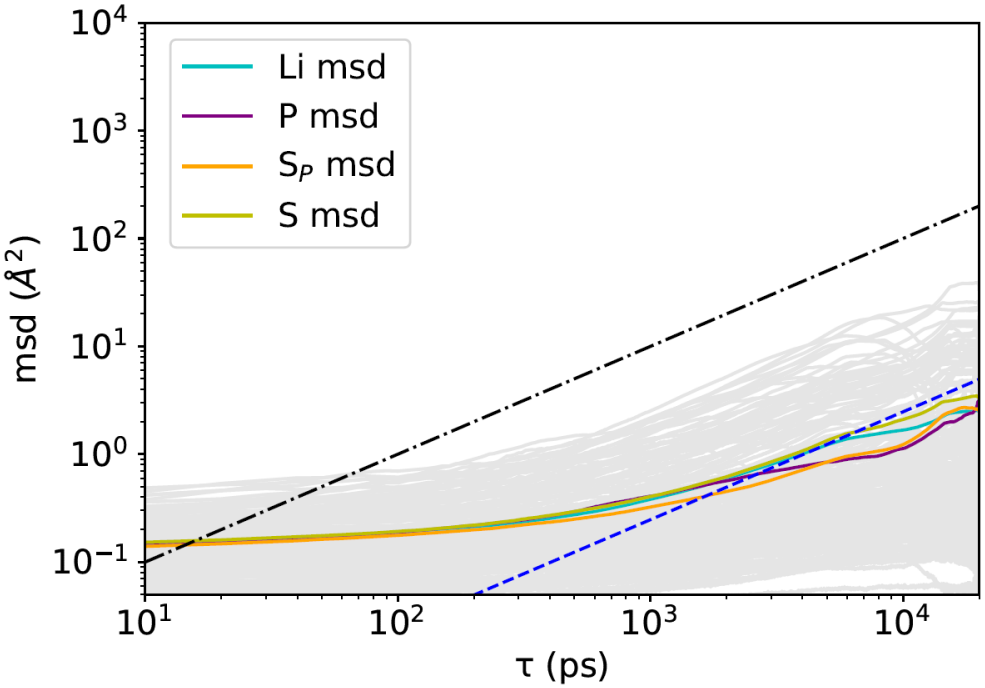

Figure S7. Ion diffusions in $Li_7(PS_4)S_2$: mean square displacement (MSD) of the species *vs.* time at room temperature (293 K). The dotted blue line has a slope of 1 leading to Fick's law of Δr^2 proportional to time. This resulted in the Li-ion diffusivity of 4.12×10^{-9} cm^2/s and Li-ion conductivity of 7.56×10^{-4} S/cm which are ~10 times lower than in $Li_6(PS_4)SCl$.

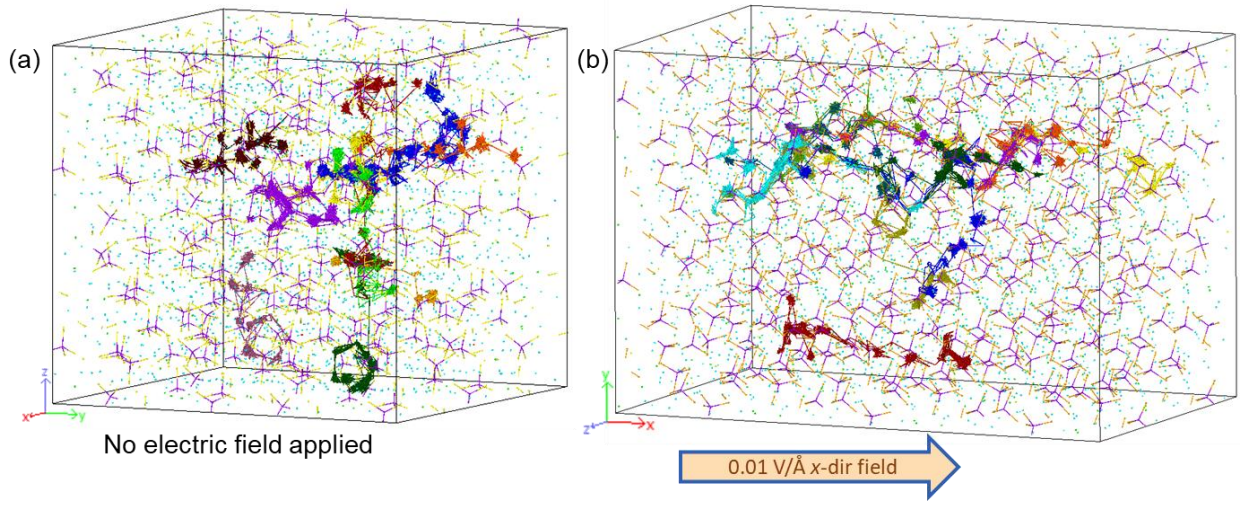

Figure S8. (a) Trajectories of 10 fastest Li-ions without electric field at 293 K. They randomly move along different directions in a 2 × 2 × 2 supercell (39.45 Å × 40.91 Å × 38.09 Å). (b) Trajectories of 10 fastest Li-ions under electric field of 0.01 V/Å along the *x*-direction. They show preferable motion along the *x*-direction in a 3 × 2 × 2 supercell (59.18 Å × 40.91 Å × 38.09 Å).

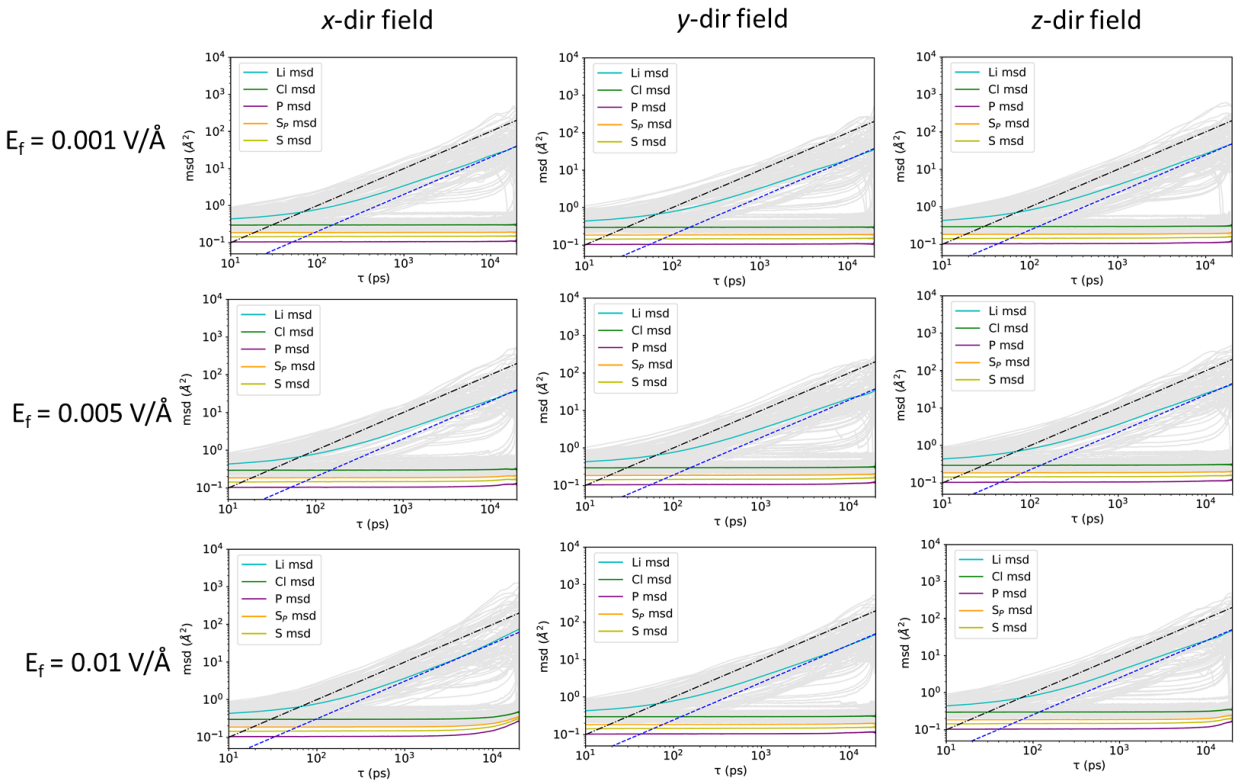

Figure S9. Trajectories of the species in $Li_6(PS_4)SCl$ under different electric field strengths at room temperature (293 K). The dotted blue lines have a slope of 1 represented by the dash-dotted black lines.

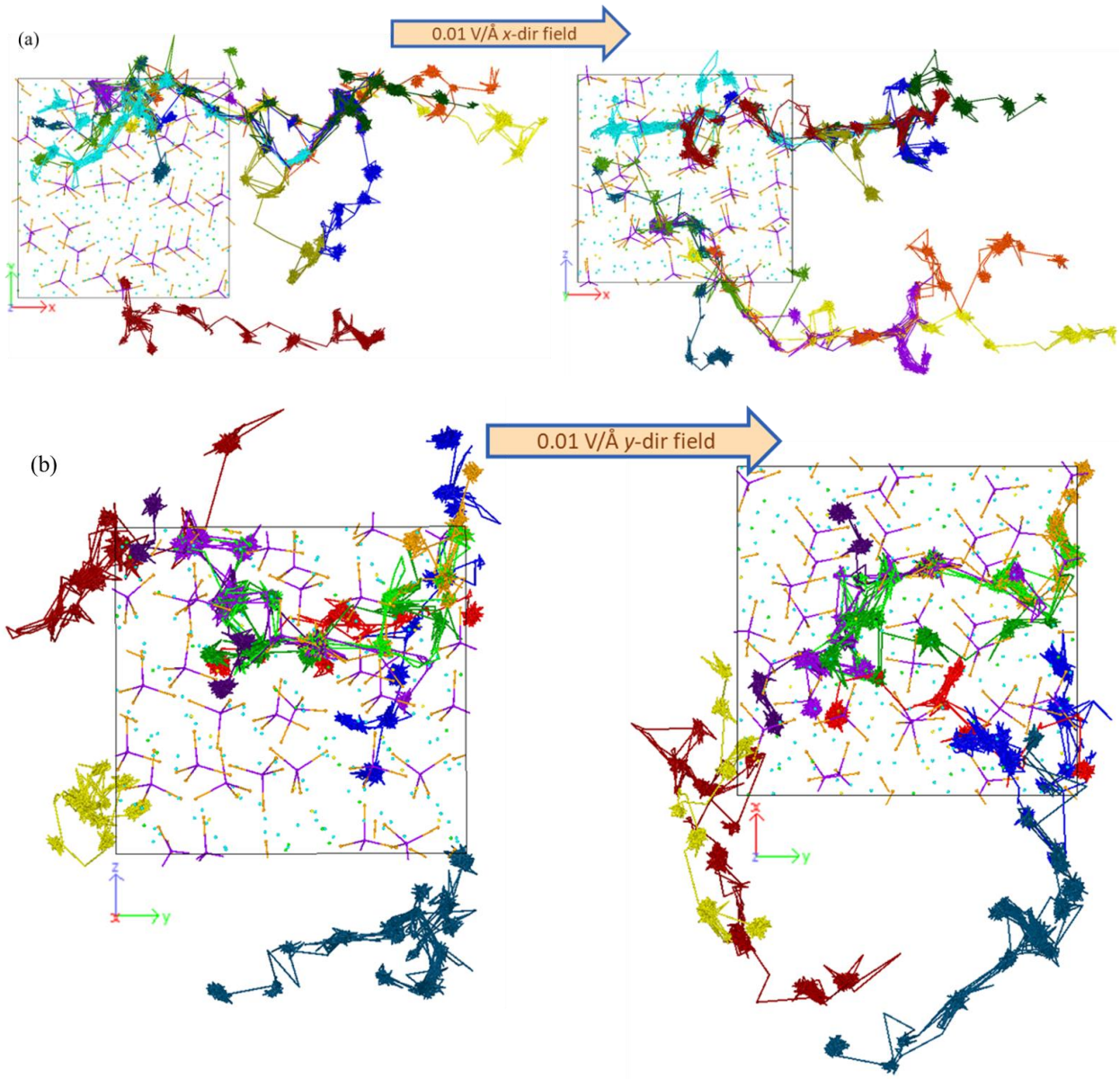

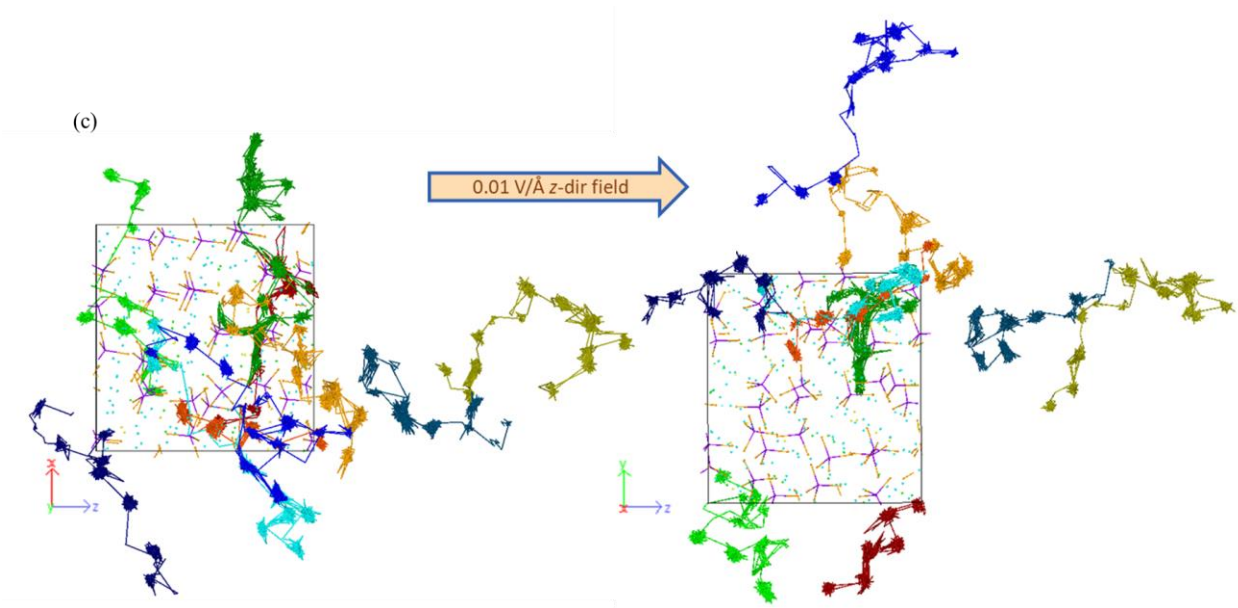

Figure S10. Trajectories of 10 fastest Li-ions over 20 ns under the 0.01 V/Å electric field applied along the (a) *x*, (b) *y*, and (c) *z* directions. Some Li-ions preferentially diffuse in (101) planes under the strong 0.01 V/Å electric field. When an electric field was applied along the *y* and *z* directions, similar preferential trajectories were observed along the 45° direction to the applied field.

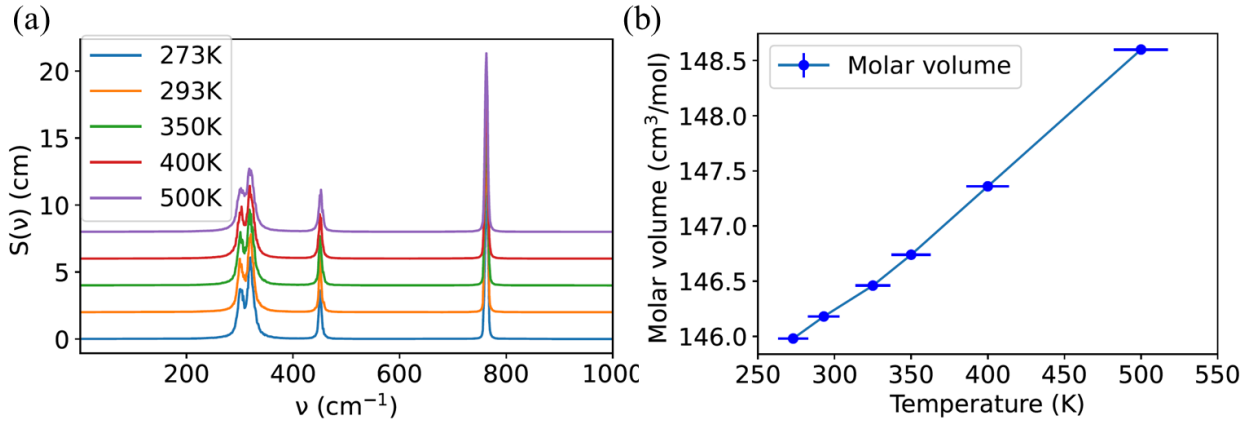

Figure S11. (a) Vibrational DoS contribution from the PS_4 tetrahedra, and (b) the molar volume predicted from one phase dynamics calculations. The same nature of the peaks at high temperatures ensures the stability of the P–S bonds with temperature. Molar volume changes linearly with temperature in a single phase. Our findings are in agreement with the change in the thermodynamic properties with temperature.

Table S1. Summary of reported experimental measurements: Li-ion conductivity and activation energy in $Li_6(PS_4)SCl$ at 298 K.

	Sample Preparation method*	Measurement Technique‡	Li-ionic conductivity (mS/cm)	Activation energy (eV)
Feng *et al.*[9]	BMA 550 ºC/ 12 hr (pellet)	EIS	7.1	0.257(7)
	BMA 460 ºC/ 12 hr ($Li_{5.3}PS_{4.3}Cl_{1.7}$) (pellet)	EIS	17.3	0.218(6)
	BMA 480 ºC/ 12 hr ($Li_{5.5}PS_{4.5}Cl_{1.5}$) (pellet)	EIS	16.1	0.221(8)
	AIMD	MSD (Einstein relation)	45	0.182
Schlenker *et al.*[10]	**commercial (powder)**	**NMR**	**3.9**	**0.28(1)**
Liu *et al.*[11]	BMA 550 ºC/ 4 hr (pellet)	EIS	6.11	0.30
	BMA 550 ºC/ 4 hr (powder)	EIS	3.50	0.33
Ganapathy *et al.*[12]	**BMA 550 ºC/ 10 hr (powder)**	**NMR**	**10.3**	**0.27(4)**
Hanghofer *et al.*[13]	**BMA 550 °C/ 7 days (pellets)**	**NMR**	**2.46**	**0.273(5)**
Yu *et al.*[14]	**SSM 550 ºC/ 10 hr (powder)**	**NMR**	**4.96**	**0.29(1)**
	BMA 550 ºC (powder)	**NMR**	**4.73**	**0.19(9)**
	SSM 550 ºC/ 10 hr (powder)	EIS	5.99	0.33(8)
	BMA 550 ºC (powder)	EIS	3.25	0.35(2)
Kraft *et al.*[15]	Hand ground + annealed 550 ºC/ 14 days (powder)	EIS	1.3	0.45(2)
Yu *et al.*[16]	**BMA 550 ºC/ 5hr (powder)**	**NMR**	**20**	**0.29(1)**
	AIMD	Transition rate	NA	0.10(1)

Rayavarapu *et al.*[17]	BMA 550 °C/ 5hr (pellet)	EIS	0.74	0.11
	BM (not annealed)	EIS	0.033	0.38
de Klerk *et al.*[18]	AIMD (50% Cl at site 4c)	MSD (Einstein relation)	40	0.17 – 0.23

*BMA - Ball milled + annealed
*SSM - Solid state method
*AIMD - *Ab initio* molecular dynamics
‡EIS - Electrochemical impedance spectroscopy
‡NMR - Nuclear magnetic resonance
‡MSD - Mean square displacement of Li-trajectories

Table S2. UFF parameters used in our LAMMPS calculations.

Pair Coefficients # lj/charmm/coul/charmm		
	D_I	X_I
Li	0.025	2.13992
Cl	0.227	3.16474
P	0.305	3.62066
S_P	0.274	3.52288
S	0.274	3.59478
Bond Coefficients # harmonic		
	K	r_0
P–S	266.873	2.06543
Angle Coefficients # cosine/squared		
	K	θ_0
S–P–S	179.88	109.471

Table S3. Atomic charge comparison from LAMMPS scaled charges *vs.* DFT calculated DDEC6 charges along with diffusivity at room temperature (293 K).[9,20]

Species	DDEC6 charge (DFT-D3)	QEq charges (LAMMPS UFF)	Scaled charge of 0.40 on Li	Scaled charge of 0.45 on Li	Scaled charge of 0.50 on Li
Li	+0.78	+0.31	+0.40	+0.45	+0.50
Cl	–0.80	–0.41	–0.41	–0.46	–0.51
PS_4	–2.26	–1.20	–1.18	–1.32	–1.46
S	–1.61	–0.27	–0.81	–0.92	–1.03
D (cm^2/s)		4.59×10^{-7}	9.8×10^{-8}	3.72×10^{-8}	9.4×10^{-9}

References:

1 G. Kresse and J. Furthmüller, *Phys. Rev. B*, 1996, **54**, 11169.

2 G. Kresse and J. Furthmüller, *Computational Materials Science*, 1996, **6**, 15.

3 G. Kresse and D. Joubert, *Phys. Rev. B*, 1999, **59**, 1758.

4 P. E. Blöchl, *Phys. Rev. B*, 1994, **50**, 17953–17979.

5 J. P. Perdew, K. Burke and M. Ernzerhof, *Phys. Rev. Lett.*, 1997, **78**, 1396.

6 S. Grimme, J. Antony, S. Ehrlich, and H. Krieg, *J. Chem. Phys.*, 2010, **132**, 154104.

7 C.-W. Lee, R. K. Behera, E. D. Wachsman, S. R. Phillpot, and S. B. Sinnott, *Phys. Rev. B*, 2011, **83**, 115418.

8 T. Das, J. D. Nicholas and Y. Qi, *J. Mater. Chem. A*, 2017, **5**, 25031.

9 T. A. Manz and N. Gabaldon Limas, RSC Adv., 2016, 6, 47771.

10 R. Schlenker, A.-L. Hansen, A. Senyshyn, T. Zinkevich, M. Knapp, T. Hupfer, H. Ehrenberg, and S. Indris, *Chem. Mater.*, 2020, **32**, 8420.

11 G. Liu, W. Weng, Z. Zhang, L. Wu, J. Yang, and X. Yao, *Nano Lett.*, 2020, **20**, 6660.

12 S. Ganapathy, C. Yu, E. R. H. van Eck, and M. Wagemaker, *ACS Energy Lett.*, 2019, **4**, 1092.

13 I. Hanghofer, M. Brinek, S. L. Eisbacher, B. Bitschnau, M. Volck, V. Hennige, I. Hanzu, D. Rettenwander, and H. M. R. Wilkening, *Phys. Chem. Chem. Phys.*, 2019, **21**, 8489.

14 C. Yu, S. Ganapathy, J. Hageman, L. van Eijck, E. R. H. van Eck, L. Zhang, T. Schwietert, S. Basak, E. M. Kelder, and M. Wagemaker, *ACS Appl. Mater. Interfaces*, 2018, **10**, 33296.

15 M. A. Kraft, S. P. Culver, M. Calderon, F. Böcher, T. Krauskopf, A. Senyshyn, C. Dietrich, A. Zevalkink, J. Janek, and W. G. Zeier, J. Am. Chem. Soc., 2017, 139, 10909.

16 C. Yu, S. Ganapathy, N. J. J. de Klerk, I. Roslon, E. R. H. van Eck, A. P. M. Kentgens, and M. Wagemaker, *J. Am. Chem. Soc.*, 2016, 138, 11192.

17 P. R. Rayavarapu, N. Sharma, V. K. Peterson, and S. Adams, *J. Solid State Electrochem.*, 2012, 16, 1807.

18 N. J. J. de Klerk, I. Rosłoń and M. Wagemaker, Chem. Mater., 2016, 28, 7955.

19 A. K. Rappe and W. A. Goddard, *J. Phys. Chem.*, 1991, 95, 3358.

20 S. Plimpton, *J. Comput. Phys.*, 1995, 117, 1.

21 R. P. Rao, N. Sharma, V. K. Peterson, and S. Adams, *Solid State Ionics*, 2013, 230, 72.

22 W. D. Jung, J.-S. Kim, S. Choi, S. Kim, M. Jeon, H.-G. Jung, K. Y. Chung, J.-H. Lee, B.-K. Kim, J.-H. Lee, and H. Kim, *Nano Lett.*, 2020, 20, 2303.